ACS APPLIED MATERIALS & INTERFACES

Research Article

Cite This: ACS Appl. Mater. Interfaces 2019, 11, 9934−9946

www.acsami.org

Evolution of the Interfacial Structure of a Catalyst Ink with the Quality of the Dispersing Solvent: A Contrast Variation Small-Angle and Ultrasmall-Angle Neutron Scattering Investigation

Rajkamal Balu,[†] Namita Roy Choudhury,*[,†] Jitendra P. Mata,[‡] Liliana de Campo,[‡] Christine Rehm,[‡,∥] Anita J. Hill,[§] and Naba K. Dutta*[,†]

[†]Chemical and Environmental Engineering, School of Engineering, RMIT University, Melbourne, Victoria 3000, Australia

[‡]Australian Centre for Neutron Scattering (ACNS), Australian Nuclear Science and Technology Organisation (ANSTO), Lucas Heights, New South Wales 2234, Australia

[∥]Guangdong Technion Israel Institute of Technology, Shantou, Guangdong Province 515063, People's Republic of China

[§]CSIRO Manufacturing, Bayview Avenue, Clayton, Victoria 3168, Australia

Supporting Information

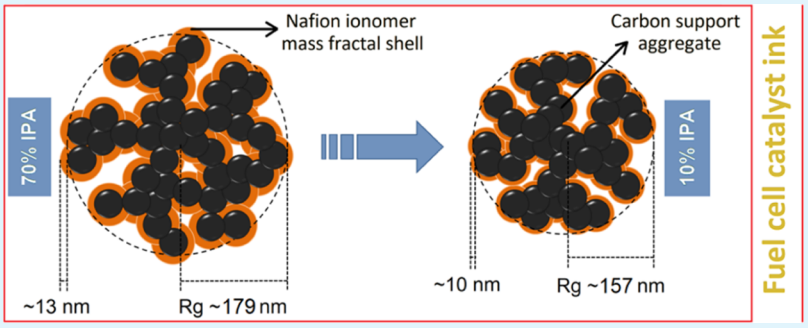

ABSTRACT: The electrocatalyst layer (ECL) of the proton-exchange membrane fuel cell (PEMFC) is commonly fabricated from colloidal catalyst ink containing carbon-supported catalyst nanoparticles (NPs), ionomer stabilizer, and dispersion medium (DM). The structure, stability, and aggregate size distribution of fuel cell catalyst ink are critically dependent on the quality of DM. However, understanding of the influence of the quality of DM on the hierarchical structure of the ECL is lacking. This work presents a systematic investigation of the effects of reducing alcohol content in isopropyl alcohol/water (IPA/H_2O) binary mixtures as DM on the structural evolution of water-rich (green) catalyst ink using contrast-variation small-angle and ultrasmall-angle neutron scattering techniques. Both qualitative and quantitative information are extracted from the data to obtain information about the size, structure, and organization of the catalyst ink using different model functions fit to the experimental data. The catalyst ink prepared using 70% IPA (commonly employed in industry and extensively reported in the literature) is shown to consist of randomly distributed globular carbon aggregates (mean radius of gyration of ∼178.9 nm) stabilized by an ionomer mass fractal shell (thickness of ∼13.0 nm), which is dispersed in the matrix of rodlike (∼1.3 nm radius and ∼35.0 nm length) negatively surface-charged ionomer NPs. These well characterized baseline data are then compared and contrasted with DM formulations of lower IPA content. A sequential reduction in IPA content of DM shows a progressive increase in the ionomer NP radius and electrostatic repulsion, concomitantly with the decrease in the carbon aggregate size and ionomer shell thickness of the catalyst ink. Therefore, the changes in the interfacial structure via adjustments of the DM composition can be used as a controlling parameter to tailor the hierarchical structure of the colloidal fuel cell catalyst ink and to further optimize the performance of the ECL.

KEYWORDS: *catalyst ink, colloidal dispersion, hierarchical structure, small-angle neutron scattering, contrast-variation, fuel cell*

INTRODUCTION

Proton-exchange membrane fuel cell (PEMFC) is one of the most promising electrochemical devices, which converts the chemical energy of hydrogen fuel directly to electricity. It is particularly advantageous for automobile applications because of its high power density, zero-emission/low pollution, and low operation temperature.[1] The heart of the PEMFC is the membrane electrode assembly (MEA), which consists of polymer electrolyte membrane, electrocatalyst layers (ECLs), and gas diffusion layers.[2] The ECL of MEA is a hierarchically structured three phase boundary at which electrochemical reaction, charge transfer, and mass transport, all occur

Received: November 24, 2018
Accepted: February 14, 2019
Published: February 14, 2019

DOI: 10.1021/acsami.8b20645
ACS Appl. Mater. Interfaces 2019, 11, 9934−9946

concurrently.[3] The ECL is commonly fabricated by air-spraying colloidal "catalyst ink", which consists of carbon-supported catalyst nanoparticles (NPs), ionomer stabilizer, and dispersion medium (DM).[4] The performance of the MEA is greatly influenced by the architecture and morphology of the ECL, which is critically dependent on the quality of the colloidal structure of the catalyst ink, the fabrication method and conditions employed.[4−6] The experimental variables associated with the design and morphology control of an ECL are large, and this control customarily relies on catalyst ink compositions that have been empirically optimized from well-tested materials such as carbon blacks, Nafion ionomers, and organic solvents. In order to mitigate the environmental impacts and risks associated with use of organic solvents, the importance of the use of water-rich (green) catalyst inks for ECL fabrication has been recognized. A few attempts have been made in the past to develop and test such green catalyst inks for fuel cell applications.[7−12] However, the colloidal structure of these green catalyst inks and the resulting hierarchical structure of the ECLs are poorly understood; this understanding is necessary to optimize and improve the performance of PEMFC.

The widely accepted microstructural model of the ECL, cast from a colloidal catalyst ink, is a hierarchical structure (multiple length scales), and this microstructure, as reported by Holdcroft,[13] consists of randomly distributed aggregates of platinum on carbon (Pt/C) NPs covered by a thin Nafion ionomer shell. The Pt/C aggregates, with intercarbon primary pores, further assemble to form larger agglomerates with secondary pores.[13] Nafion is a perfluorinated ionomer, which consists of a hydrophobic perfluoroethylene backbone with perfluorinated vinyl ether side chains terminated with hydrophilic sulfonic acid groups.[14] Classical molecular dynamic simulations have shown that the thin Nafion ionomer film covering Pt/C aggregates in fuel cell catalyst ink is irregular, and the densely arranged charged side chains of the ionomer form a highly ordered array on the film surface.[15,16] Recently, in some elegant electron tomography work, Lopez-Haro et al.[17] studied the local 3D structure of a fuel cell ECL and showed that doubling the amount of the Nafion ionomer in the electrode led to a two-fold increase in its degree of coverage of the carbon, whilst the average thickness of the ionomer layer (∼7.0 nm) remained unchanged.[17] Moreover, ultrathin (<55.0 nm) films of the Nafion ionomer have been reported as showing enhanced surface polarity leading to high electron-accepting and/or proton-donating properties in aqueous solutions.[18] Nevertheless, the morphology and distribution of Pt/C aggregates and Nafion ionomer in the ECL, and the resultant fuel cell performance of the fabricated MEA, are dependent on the structure of the colloidal catalyst ink, which in turn depends critically on the polarity/dielectric constant and surface tension of DM used for catalyst ink preparation.[10,19] DMs commonly used for catalyst ink preparation are organic solvent-based formulations.[20,21] Particularly, 70% propanols are the most commonly employed DM in the industry and are extensively reported in literature.[8,22] Recently, Takahashi et al.[23] studied the local structure of an *n*-propyl alcohol-based catalyst ink dispersion using cryo-transmission electron microscopy (TEM), which showed rodlike Nafion ionomer NPs and Pt/C aggregates (>200.0 nm). The rodlike colloidal structure of Nafion ionomer NPs in alcohol-based DMs has also been reported using small-angle scattering (SAS) techniques.[24,25] The hierarchical structure and organization of colloidal fuel cell catalyst inks from nano- to microscale are not well understood, largely because of limitations of the techniques that have been previously used and the dynamic and heterogeneous nature of the catalyst dispersion.[13] SAS is a powerful technique of choice for investigating colloidal structures from 10 Å to 10 μm.[26] Few attempts have been made to characterize the structure of fuel cell catalyst inks using SAS techniques such as small-angle X-ray scattering (SAXS) and small-angle neutron scattering (SANS), and these studies have been limited to alcohol-rich DMs.[27−30]

In recent years, ECLs fabricated from water-rich catalyst ink dispersions have been reported to lead to enhanced mass transport properties and efficiencies in the performance of PEMFC.[10−12] The superior performance of ECLs fabricated from water-rich DMs, as compared to alcohol-rich DMs, is hypothesized to arise from structural differences in the colloidal catalyst inks. In this investigation, both contrast-variation SANS (CV-SANS) and contrast-variation ultra-SANS (CV-USANS) are used for the first time to study the structural organization of fuel cell catalyst ink dispersions prepared using isopropyl alcohol/water (IPA/H_2O) mixtures as DM with the range of IPA content from 10 to 70%. As such, this study investigates ink formulations that are commensurate with currently commercial inks (20−35% water) as well as novel inks that are green having ≥50% water. SANS is a powerful technique for investigating the nanostructure and organization of proteins, synthetic polymers, and inorganic colloidal dispersions.[31,32] Moreover, SANS is complementary to electron microscopy and SAXS, and is sensitive to lighter elements such as hydrogen, which gives the unique opportunity of contrast matching.[32] The contrast-variation/matching capability of neutron scattering is particularly advantageous for studying the structure of multicomponent systems such as catalyst ink, where the total scattering intensity can be deconvoluted into scattering functions corresponding to the structure of individual components present in the system.[30] Furthermore, the use of USANS allows structural characterization of colloidal aggregates up to several microns.[33] Combining SANS and USANS including the contrast-variation technique enables the first systematic exploration of the colloidal structure of green catalyst inks over a wide length scale (10 Å to 10 μm).

MATERIALS AND METHODS

Materials. Chloroplatinic acid hydrate, sodium hydroxide (NaOH), phosphate buffered saline (PBS)—pH 7.4, sodium borohydride ($NaBH_4$), and IPA were purchased from Sigma-Aldrich, Australia. Vulcan XC-72-R carbon powder and Nafion ionomer dispersion (equivalent weight of 1100) were purchased from Fuel Cell Earth, USA, and used as received. Milli-Q water (H_2O), deuterium oxide (D_2O), and deuterated IPA (IPA-*d*) were supplied by the Australian Nuclear Science and Technology Organization (ANSTO).

Dynamic Light Scattering. The zeta (ζ) potential and hydrodynamic diameter (D_h) of the Nafion ionomer and carbon support in IPA/H_2O mixtures as DM were experimentally determined by the dynamic light scattering (DLS) technique using a Zetasizer (NanoZS, Malvern Instruments Ltd.). The measurements were performed at a fixed temperature of 20 °C with respective DM parameters (dielectric constant and viscosity) recorded in the Zetasizer software. The ζ-potential values were determined from the measured electrophoretic mobility (μ) using the Smoluchowski approximation (eq 1) using the DTS Nano software, which runs algorithm based upon a nonnegative least-squares fit[34]

$$\mu = \frac{\zeta \varepsilon V}{4\pi\eta D} \tag{1}$$

where V is the applied voltage, D is the electrode separation; ε and η are the dielectric constant and viscosity of DM, respectively. The measured

DOI: 10.1021/acsami.8b20645
ACS Appl. Mater. Interfaces 2019, 11, 9934−9946

D_h and ζ-potential values were calculated from cumulative analysis of three cycles.

Fuel Cell Catalyst Powder Preparation. The fuel cell catalyst powder (40 wt % Pt on Vulcan XC72) was prepared by our patented method using *Rec1-resilin* as the directing and stabilizing agent.[35] *Rec1-resilin* is a bio-mimetic,[36] multiresponsive,[37−39] and intrinsically disordered protein polymer[31,40] synthesized using a cloning approach as reported previously.[41] For Pt-NPs synthesis, 1 M aqueous NaOH was first added dropwise to 300 mL of 10 mM aqueous PBS containing *Rec1-resilin* (0.579 μM) to obtain a solution with pH of ∼12. About 100 mL of 2.4 mM chloroplatinic acid (precursor) was added drop wise to the protein solution under stirring. The protein-precursor mixture was then equilibrated for 30 min at ∼12 °C, and 25 mL of freshly prepared 24 mM $NaBH_4$ was introduced under stirring. After 5 min of stirring, the solution mixture was equilibrated for 15 min at ambient temperature without stirring. Change in solution color from pale yellow to light brown indicates generation of Pt-NPs. For Pt/C catalyst NP synthesis, 1 mg/mL Vulcan carbon was first dispersed in the 1:13 IPA:H_2O (v/v) solution mixture using an ultrasonicator (Qsonica, model Q125, USA) operated at 40% amplitude for 1 h with an ON and OFF cycle of 60 and 30 s, respectively. The temperature of the dispersion was maintained at 20 °C. The carbon dispersion was then added drop wise to the protein-stabilized Pt-NPs dispersion under stirring for 1 h to obtain a 40 wt % Pt loading on Vulcan carbon. The obtained Pt/C fuel cell catalyst dispersion was then centrifuged at 14 000 rpm for 10 min, and the pellet was washed several times with Milli-Q water by subsequent redispersion and centrifugation. The washed pellet was then vacuum-dried overnight at 40 °C to obtain the dry Pt/C catalyst powder.

Fuel Cell Catalyst Ink Preparation. The fuel cell catalyst ink was prepared using IPA/H_2O mixtures as DM. IPA contents of 10, 30, 50, and 70% by volume were used in DM. The samples were prepared by first dispersing a desired amount of Pt/C catalyst powder in DM under sonication. After 5 min of sonication, a measured volume of the Nafion ionomer was added drop wise to the above dispersion under sonication. The typical solid content of the catalyst ink was 1.0 wt %; where the Nafion ionomer contributed 0.3 wt %. The dispersion mixture was then ultrasonicated for 1 h with an ON and OFF cycle for 60 and 30 s, respectively. The temperature of the dispersion was maintained at 20 °C in all cases. The obtained black catalyst ink dispersion was used for structure analysis.

Contrast-Variation SANS. CV-SANS analysis was performed using the Quokka SANS instrument.[42] Source aperture to sample aperture distances of 2, 12, and 20 m with a neutron wavelength of 5 and 8.1 Å (for 20 m lens optics), respectively, were employed to cover the scattering vector, q, (eq 2) in the range of 0.0007−0.39 $Å^{-1}$.[43]

$$q = \frac{4\pi \sin\theta}{\lambda} \tag{2}$$

where θ is the angle of scattering and λ is the wavelength of neutrons. The Vulcan carbon and Nafion ionomer have a neutron scattering length density (SLD) of ∼6.20 × 10^{-6} and ∼3.25 × 10^{-6} $Å^{-2}$, respectively.[29] The neutron SLD of H_2O, IPA, D_2O, and IPA-*d* were calculated to be −0.56 × 10^{-6}, −0.33 × 10^{-6}, 6.36 × 10^{-6}, and 6.23 × 10^{-6} $Å^{-2}$, respectively, using the National Institute of Standards and Technology (NIST, USA) neutron activation and scattering calculator (https://www.ncnr.nist.gov/resources/activation/). For Nafion ionomer experiments, IPA-*d*/D_2O mixtures were used as DM. For catalyst ink experiments without contrast-matching, IPA/H_2O mixtures were used as DM. For catalyst ink experiments with Nafion ionomer contrast-matching, mixture of deuterated and hydrogenous solvents (i.e., partially deuterated IPA/H_2O mixtures) were used as DM. For catalyst ink experiments with carbon contrast-matching, IPA-d/D_2O mixtures were used as DM. For structure analysis, the prepared dispersions were loaded into demountable Quokka cells of 20.0 mm diameter and 1.0 mm path length. The cell temperature was maintained at 20 °C for all measurements. SANS data were reduced using NCNR SANS reduction macros (modified for the Quokka instrument) using the Igor software package with data corrected for empty cell scattering and transmission.[44] Data collected were transformed to absolute scale using an attenuated direct beam transmission measurement. In all the cases, the appropriate buffer backgrounds were subtracted from the sample scattering using the PRIMUS computer program.[45]

Contrast-Variation Ultrasmall-angle Neutron Scattering. CV-USANS analysis was performed using the Kookaburra USANS instrument using the long neutron wavelength configuration (λ = 4.74 Å).[46] The scattering data were collected at room temperature in the q range of 0.00007−0.003 $Å^{-1}$. For structure analysis, the dispersions prepared for SANS analysis were loaded into demountable Kookaburra cells of 35.0 mm diameter and 0.5 mm path length. The raw USANS data of the samples collected from the respective empty cells (background) were reduced using scattering and converted to the absolute scale using python scripts based on the standard procedure.[46] The experimental data were desmeared using the Lake algorithm, incorporated in the NIST USANS macros, and the data were finally merged with the SANS data for analysis using the Igor Pro computer program.[44] The incoherent background scattering from samples was determined with a high-q power law fit using the SasView computer program (https://www.sasview.org/) and subtracted from the respective data for analysis.[47] The structural parameters of the samples were determined by fitting the combined SANS and USANS data with selective model functions using the SasView computer program.

RESULTS AND DISCUSSION

Structural Evolution of Ionomer with DM. In order to study the structure and organization of colloidal fuel cell catalyst inks containing Pt/C NPs and Nafion ionomer in water-rich DMs, it is crucial to understand the structure of the colloidal Nafion ionomer in the range of DM formulations. The measured ζ-potential and D_h values of the Nafion ionomer in IPA/H_2O mixtures as DM along with the dielectric constant and surface tension of IPA/H_2O mixtures (reported in literature)[48,49] are given in Figure 1. Several models including spherical clusters, bundle, ribbon, bilayer, network, and disordered and parallel cylinder have been proposed to explain the structure of the hydrated Nafion ionomer in the literature, and the parallel cylinder water nanochannel model has been the most popular during the last decade.[14,50] The parallel cylinder water nanochannel model depicts the structure of the hydrated Nafion ionomer as inverted-micelle cylinder NPs with the hydrophobic polymer backbone on the outside and the ionic side groups lining the water channel inside, which further self-assembles into hexagonal arrays.[50] However, recently Paul et al.[18] demonstrated that the cylindrical Nafion ionomer NPs exhibit distinct surface characteristics based on their concentration in alcohol/water mixtures as DM. The authors reported that the Nafion ionomer NPs exhibit hydrophilic surfaces (hydrophobic polymer backbones on the inside and the ionic side groups on the outside) at concentrations less than 1.0 wt % and hydrophobic surfaces (hydrophobic polymer backbones on the outside and the ionic side groups on the inside) at concentrations greater than 1.0 wt %, similar to that reported for Nafion membranes.[18,50] The interaction energies between colloidal particles suspended in a DM include attractive van der Waals (arising from dipole−dipole interactions), repulsive electrostatic/Coulombic (arising from electric double layer and surface potential), steric hindrance (caused by an attached polymer chain), and hydrophobic interaction.[51] The measured negative ζ-potential (Figure 1) supports the reported rodlike micellar structure of Nafion ionomer NPs with hydrophobic polymer backbone on the inside and the ionic side groups on the outside.[18] As the pK_a value of sulfonate end groups of Nafion is ∼6, the sulfonic acid end groups are fully dissociated (SO_3^-) in IPA/H_2O mixtures (pH ∼7) giving negative surface charge to Nafion ionomer NPs.[52] The observed increase in ζ-potential with the decrease in

DOI: 10.1021/acsami.8b20645
ACS Appl. Mater. Interfaces 2019, 11, 9934−9946

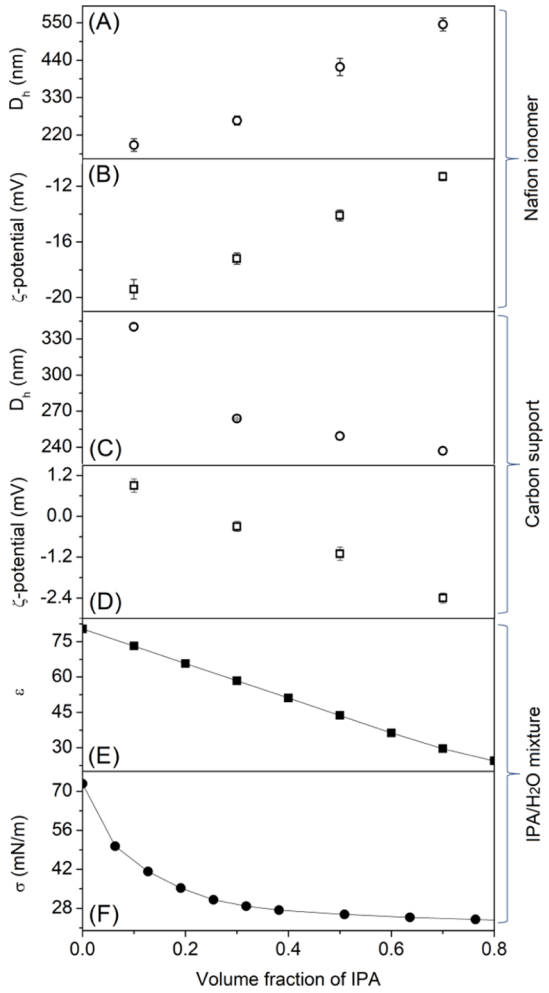

Figure 1. (A,C) are hydrodynamic diameter (D_h), and (B,D) are zeta (ζ) potential of the Nafion ionomer and carbon support, respectively, in IPA/H_2O mixtures as DM. Each sample was measured thrice to calculate average and standard deviation. (E) Dielectric constant (ε) and (F) Surface tension (σ) of IPA/H_2O mixtures from literature.[48,49]

IPA content in the DM could be due to two factors: (i) an increased amount of sulfonic acid end group diffusion at the polymer−solvent interface (side chain extension) because of the sulfonate interaction with water molecules and (ii) the decrease in IPA content increases the dielectric constant (polarity) of DM.[53] The sulfonic acid group in the Nafion ionomer has a high water-of-hydration, absorbing around 20 water molecules for every acid group in the Nafion ionomer.[54] The radius and length of rodlike Nafion ionomer NPs are reported to be around 2.4 and 40.0 nm, respectively, in alcohol/water mixtures as DM.[24,55] Moreover, even at low concentrations (<1 wt %), the rodlike Nafion ionomer NPs have been reported to have a tendency to aggregate, which has been attributed to the strong hydrophobic interaction of the fluorocarbon backbone.[56] Therefore, the D_h of the Nafion ionomer (Figure 1) measured using DLS is expected to be their NP aggregate structures. The observed decrease in D_h of Nafion ionomer NP aggregates with progressive decrease in IPA content in DM is resulting from increased electrostatic repulsion related to increase in negative ζ-potential of ionomer NPs.[57] On the other hand, the ζ-potential of the hydrophobic carbon support (Figure 1) was observed to decrease, whereas the D_h to increase with decrease in IPA content in DM. In a suspension with no additional ionic species, particle surface charge comes from either electron transfer between DM molecules and the surface, or surface ionic group dissociation, or preferential dissolution.[58] Carbon black particles consist of thousands of microstructures with π conjugation in disrupted concentric arrangement, and the carbon atoms at the edges of each microstructure may bond with hydrogen and oxygen-containing groups via the Lewis acid−base interaction between the particle surface and DM molecules leading to the particle surface charge.[58,59] In IPA-based DM, carbon black behaves as a Lewis acid receiving electron pairs from DM, and therefore exhibits negative ζ-potential, whereas vice versa in H_2O.[58] The observed ζ-potential of the carbon support in IPA/H_2O mixtures as DM is in general agreement with literature reports.[58]

Figure 2 shows the SANS intensity profile of the Nafion ionomer (0.3 wt %) in IPA-d/D_2O mixtures as DM and their respective model function fits. SANS experiments on the Nafion ionomer were performed using deuterated solvents in order to obtain good contrast, while minimizing incoherent scattering from the system. The overall neutron scattering intensity, $I(q)$ of colloidal dispersion is expected to be a function of both the form factor ($P(q)$)—an intramolecular scattering event, and the structure factor ($S(q)$)—an intermolecular scattering event, as given in eq 3[60]

$$I(q) = \varphi P(q) S(q) \tag{3}$$

where φ is a scaling factor related to the difference in neutron SLD and the volume of scatterers. The $P(q)$ contains information about the distribution of interatomic distances within a molecule and can be interpreted in terms of its size and shape; whereas $S(q)$ provides information about the orientation-averaged particle−particle interactions and can be interpreted in terms of interparticle distance and/or spatial distribution.[61,62] The explicit form of all model functions used in modeling the data are given in the Supporting Information. The SANS intensity profile of the Nafion ionomer (Figure 2A) in different DMs, within the experimental range showed three distinctive scattering regions: a high-q Porod region ($0.08 < q < 0.3$ Å^{-1}), a mid-q Guinier region ($0.025 < q < 0.08$ Å^{-1}), and a low-q correlation length region ($0.008 < q < 0.01$ Å^{-1}). The high-q and mid-q regions are attributed to the intramolecular scattering (illustrated by asymptotic behavior), whereas the low-q regime is dominated by intermolecular scattering (illustrated by local maximum or peak).[62] The scattering intensity of the Nafion ionomer at mid-q and/or low-q was observed to increase with decrease in IPA content in DM, suggesting increase in size and/or aggregation on this length scale. The maximum observed in the low-q region is hypothesized to arise from the spatial distribution of the Nafion ionomer NP in DM, which is further supported by the Kratky plot (Figure 2B) clearly showing the correlation peak corresponding to Nafion inter-NP distance in the low-q region followed by a slight increase in slope and/or plateau corresponding to the intrinsic structure of the Nafion ionomer in the mid-q and high-q regime.[43,63]

The SANS intensity profiles of the Nafion ionomer were fitted (Figure 2C) with the cylinder $P(q)$ model.[64] The cylinder model was considered to be uniquely appropriate and applied for data fitting as the structure of Nafion molecules in alcohol-based aqueous DM has been argued in literature as "rodlike" based on TEM, SAXS, SANS, and nuclear magnetic resonance studies.[23−25,56] Moreover, a slope value of ∼1.0 (Figure 2A) obtained from the power law fit in the mid-q region ($0.03 < q < 0.06$ Å^{-1}) of the SANS profile supports the presence of the rodlike (cylinder) structure.[63] The cylinder model calculates the

DOI: 10.1021/acsami.8b20645
ACS Appl. Mater. Interfaces 2019, 11, 9934−9946

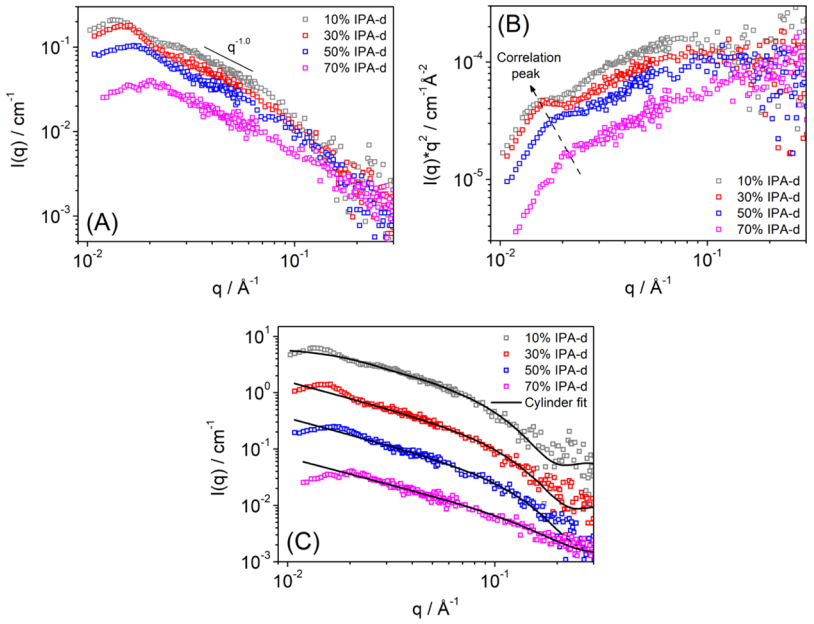

Figure 2. (A) SANS intensity profile and (B) Kratky plot of the Nafion ionomer in IPA-d/D_2O mixtures as DM. (C) Cylinder model function fit to the respective SANS data presented as intensity offsets for clarity.

radius and length of randomly oriented cylinders in DM. In principle, the length of cylindrical Nafion ionomer NPs could be estimated from SANS data from the onset of changes in q-dependence of $I(q)$ from q^0 to q^{-1}. However, the exact length of the cylindrical Nafion ionomer NPs in IPA-d/D_2O mixtures as DM could not be estimated because of the interference of the correlation peak at low-q, which conceals the onset of changes in q-dependence. A similar observation has been previously reported by Yamaguchi et al.[25] for Nafion ionomer NPs in alcohol/H_2O mixtures as DM, where the length of the cylinder was assumed to be infinitively long to estimate the radius of the NPs. Nevertheless, the cylinder model fit of the Nafion ionomer in the 10% IPA-d/D_2O mixture as DM (Figure S1 in Supporting Information) returned a cylinder length of ∼25.9 nm for the measured q-range ($0.01 < q < 0.3$ Å^{-1}) and ∼32.8 for the limited q-range ($0.025 < q < 0.3$ Å^{-1}), which are within the range of values reported for the dilute Nafion ionomer in alcohol/H_2O mixtures as DM.[24,56] Recently, Welch et al.[65] reported the cylindrical length of the Nafion ionomer NPs in 100% IPA DM to be ∼35.0 nm. Therefore, we attempted to estimate the radius of the cylindrical Nafion ionomer NPs in 10% IPA-d/D_2O mixture as DM by fitting the data with the cylinder model in the measured q-range fixing the length to 25.9 and/or 35.0 nm. The standard deviation of the resulting radius values was less than 5% suggesting no significant difference in the obtained radius. Therefore, the length of cylindrical Nafion ionomer NPs was fixed to 35.0 nm in the SasView program in order to obtain the fitted radius of the NPs for all samples (Figure S2 in Supporting Information). The structural parameters of Nafion ionomer NPs estimated from model function fits are given in Table 1. The radius of cylindrical Nafion ionomer NPs was observed to increase progressively from ∼1.3 to ∼1.8 nm with decrease in IPA-d content (from 70 to 10%, respectively) in IPA-d/D_2O mixtures as DM, demonstrating that the packing density of the material along the perfluorocarbon backbone increases. This could be driven by the increased repulsion between perfluorocarbons and DM from alcohol-rich to water-rich DMs that result in need for improved interface minimization and improved interface coverage by hydrophilic groups. On the other hand, the side chains may stretch out going from alcohol-rich to water-rich DMs, so that the radius increases and the length decreases.[24] For a system of charged particles with screened Coulombic repulsion in a dielectric medium, the $S(q)$ can be calculated using the Hayter–Penfold rescaled MSA model; however, it is appropriate only for spherical or ellipsoidal particles.[64] Therefore, the mean interparticle distance (d) of the rodlike Nafion ionomer NPs was estimated from the correlation peak value using the relation $d = 2\pi/q$ (Table 1).[66] Nafion ionomer inter-NP distance was observed to increase progressively from ∼29.1 to ∼44.3 nm with decrease in IPA-d content (from 70 to 10%, respectively) in IPA-d/D_2O mixtures as DM. The increase in Nafion ionomer inter-NP distance going from alcohol-rich to water-rich DM could be due to increased electrostatic repulsion resulting from the increase in negative ζ-potential of ionomer NPs.[51,57] A schematic of the Nafion ionomer structure in IPA/H_2O mixtures as DM is given in Figure 3.

Evolution of SANS Profile with Individual Contrast Match. The contrast-variation capability of neutron scattering provides a unique opportunity to study the structure of individual components in multicomponent systems such as catalyst ink dispersions, where the scattering intensity of desired components can be masked to obtain the scattering from another.[30] Figure 4A shows the SANS intensity profile of the catalyst ink prepared using DM with different contrast-matching conditions (without contrast-match, and carbon/Nafion contrast-matched). It can be clearly observed from the figure that the contrast-matching carbon support or Nafion ionomer reduces the overall scattering intensity of the catalyst ink, providing structural information of one component masking the other. The scattering contribution from Pt-NPs and *Rec1-resilin* on the carbon support in the catalyst ink is very low or negligible because of their very small volume fraction (0.0001 and 0.0002, respectively) compared to the carbon support (0.0064), Nafion ionomer content (0.0032), and DM (0.9901).[29,35] The scattering intensity profiles of the catalyst ink within the

DOI: 10.1021/acsami.8b20645
ACS Appl. Mater. Interfaces 2019, 11, 9934–9946

Table 1. Structural Parameters of the Nafion Ionomer, Carbon Support, and Catalyst Ink

method	sample	scattering profile	[a]model function fitting	structural parameters	70 vol %	50 vol %	30 vol %	10 vol %	DM neutron SLD ($\times 10^{-6}$ Å^{-2})	DM contrast matching conditions
					IPA content in the DM					
[b]DLS	Nafion ionomer	Figure 1		D_h of Nafion ionomer NP aggregates (nm)	545 ± 19	420 ± 25	262 ± 13	190 ± 18		
	carbon support			D_h of carbon aggregates (nm)	237 ± 3	249 ± 3	264 ± 1	340 ± 3		
[c]SANS and USANS	Nafion ionomer	Figure 2	cylinder	radius of Nafion ionomer NPs (nm)	1.3 ± 0.0	1.5 ± 0.0	1.7 ± 0.1	1.8 ± 0.1	6.26−6.36	carbon contrast match
				Nafion ionomer inter-NP distance (nm)	29.1 ± 0.2	35.2 ± 0.2	40.1 ± 0.1	44.3 ± 0.1		
	catalyst ink	Figure 5	Guinier−Porod	R_g of carbon aggregates (nm) in catalyst ink	178.9 ± 1.2	170.3 ± 1.1	165.0 ± 1.1	156.5 ± 1.1	3.25	Nafion contrast match
				Dimension variable	0.013 ± 0.010	0.013 ± 0.010	0.012 ± 0.010	0.012 ± 0.010		
		Figure 6	Guinier−Porod + cylinder	R_g of carbon aggregate−Nafion ionomer particles in catalyst ink (nm)	191.9 ± 2.6	182.4 ± 1.7	176.1 ± 1.1	166.2 ± 1.8	−0.40 to −0.54	without contrast match
				dimension variable	0.014 ± 0.002	0.014 ± 0.010	0.012 ± 0.011	0.011 ± 0.010		
				Nafion ionomer shell thickness in catalyst ink (nm)	∼13.0	∼12.1	∼11.1	∼9.7		
		Figure 7	Guinier−Porod + cylinder	R_g of Nafion ionomer mass fractal in catalyst ink (nm)	192.1 ± 2.6	185.4 ± 7.5	179.2 ± 5.4	168.2 ± 4.3	6.26−6.36	carbon contrast match
				fractal dimension	2.51 ± 0.01	2.62 ± 0.01	2.62 ± 0.01	2.62 ± 0.01		

[a]Explicit form of the model functions and all other parameters used for data fitting are given in Supporting Information. [b]Standard deviation values for DLS experiments were calculated from three repeat measurement cycles. [c]Standard deviation values for SANS and USANS experiments were obtained from respective model fitting, which depends on number of fixed and fitted parameters.

ACS Appl. Mater. Interfaces 2019, 11, 9934−9946
DOI: 10.1021/acsami.8b20645

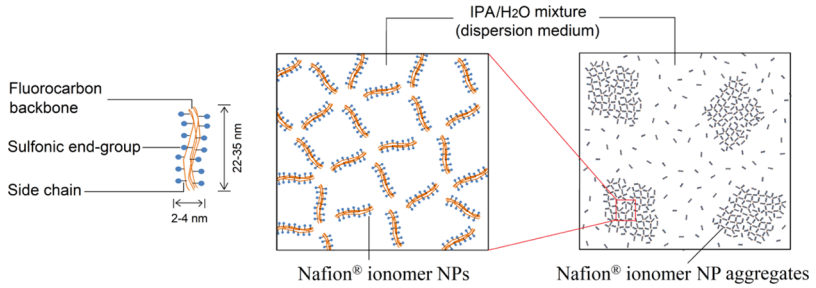

Figure 3. Schematic illustration of the structure of the Nafion ionomer in IPA/H_2O mixtures as DM.

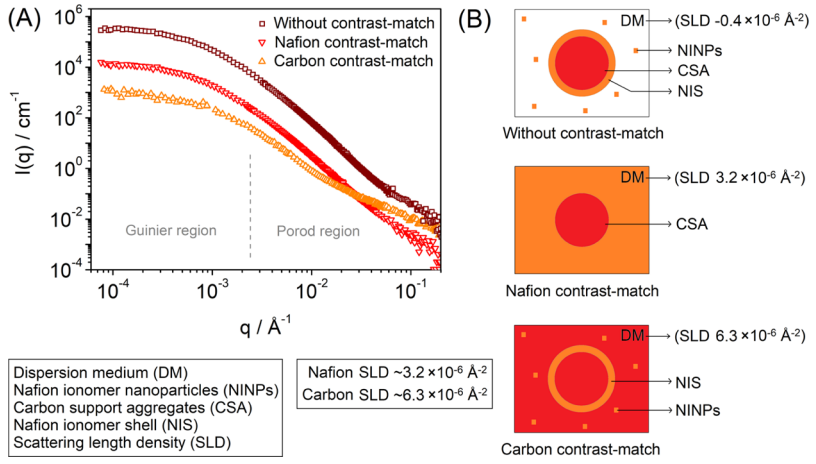

Figure 4. (A) SANS intensity profile of fuel cell catalyst ink prepared using 70% IPA/H_2O (without contrast-match), partially deuterated 70% IPA/H_2O (Nafion contrast-matched), and 70% IPA-*d*/D_2O (carbon contrast-matched) mixtures as DM. (B) Schematic of structures visible or providing scattering contrast in catalyst ink at different contrast-matching conditions of DM.

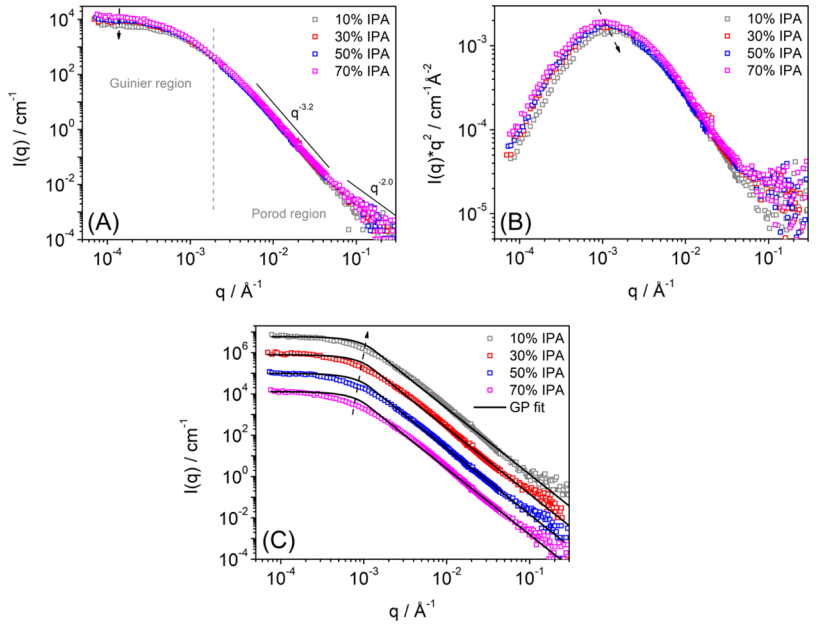

Figure 5. (A) SANS and USANS combined intensity profile and (B) Kratky plot of fuel cell catalyst ink prepared using partially deuterated IPA/H_2O mixtures (Nafion contrast-matched) as DM. (C) GP model fits of respective scattering data presented as intensity offsets for clarity. The arrows in (A–C) show the decrease in low-*q* intensity, shift in peak maximum, and shift in turnover point of the Guinier region, respectively, with decrease in alcohol content in DM.

experimental range showed two major regions: a high-*q* to mid-*q* Porod region ($0.002 < q < 0.3$ Å^{-1}) and a low-*q* Guinier region ($0.00007 < q < 0.002$ Å^{-1}). The Porod region could provide the quality of the interface (carbon–Nafion–DM or carbon–DM or Nafion–DM), whereas the Guinier region could provide the size of formed colloidal structures (carbon–Nafion ionomer or carbon or Nafion ionomer).[26] A schematic of structures visible or providing scattering contrast in the catalyst ink at different

DOI: 10.1021/acsami.8b20645
ACS Appl. Mater. Interfaces 2019, 11, 9934–9946

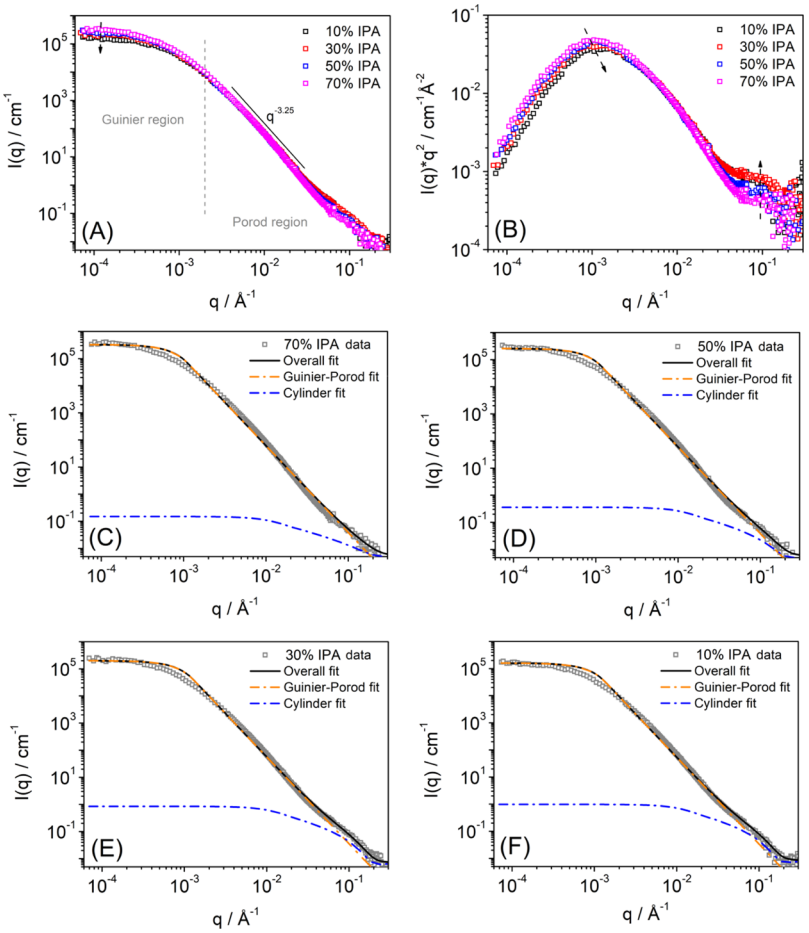

Figure 6. (A) SANS and USANS combined intensity profile and (B) Kratky plot of fuel cell catalyst inks prepared using IPA/H_2O mixtures (without contrast-match) as DM. (C–F) are model function fits of respective scattering data. The arrows in (A,B) show decrease in low-q intensity, shift in peak maximum, and increase in high-q intensity, respectively with decrease in alcohol content in DM.

contrast-matching conditions of DM is shown in Figure 4B. Performing such contrast-matching experiments at various solvent ratios in DM provides the opportunity to study the effect of solvent quality on the structural evolution of water-rich catalyst inks for PEMFC.

Evolution of Hierarchical Structure of Carbon Support with DM. Figure 5 shows the double logarithmic SANS and USANS combined intensity profile of catalyst inks prepared using partially deuterated IPA/H_2O mixtures (Nafion contrast-matched) as DM (i.e., a mixture of deuterated and hydrogenous solvents was used to adjust the neutron SLD of DM to match that of the Nafion ionomer), and their respective model function fits over a wide q-range (0.00007–0.3 Å^{-1}). Such plots enable elucidation of the hierarchical structure of the carbon support in catalyst ink dispersions. The scattering intensity profile of the carbon support (Figure 5A) within the experimental range showed three distinctive regions: a high-q Porod region ($0.08 < q < 0.3$ Å^{-1}), a mid-q Porod region ($0.002 < q < 0.08$ Å^{-1}), and a low-q Guinier region ($0.00007 < q < 0.002$ Å^{-1}). The carbon support (Vulcan XC72) has an average diameter of ∼50.0 nm (provided by the supplier). For a spherical particle of 50.0 nm diameter, the turnover point in the Guinier region is expected to be observed at the mid-q region ($q \approx 0.01$ Å^{-1}).[63] Therefore, the observed turnover point of the Guinier region of Nafion contrast-matched catalyst ink at low-q ($0.00007 < q < 0.002$ Å^{-1}) suggests that the carbon support is present as aggregates in catalyst ink. The scattering intensity of the carbon support at low-q was observed to decrease, suggesting decrease in the size of carbon aggregates with decrease in IPA content in DM. Moreover, the Kratky plot (Figure 5B) showed a slight shift in the peak maximum toward the higher q-value supporting the decrease in size of the carbon aggregates with decrease in IPA content in DM.[43,63] The scattering data fit with a power law function in the high-q Porod region ($0.08 < q < 0.3$ Å^{-1}) resulted in a slope value of ∼2 for all samples (Figure 5A), which can be attributed to the intracarbon NP structure/pores.[67] The scattering data fit with a power law function in the mid-q Porod region ($0.006 < q < 0.02$ Å^{-1}) resulted in a slope value of ∼3.2 for all samples (Figure 5A), which corresponds to the surface roughness (porous surface) of carbon NPs in dilute solvent-based DM.[28,63,67] In order to determine an appropriate model for estimating structural parameters of catalyst ink, the scattering data of catalyst ink prepared using partially deuterated 70% IPA/H_2O (Nafion contrast-matched) mixture as DM was fitted with different shape-independent model functions including mass fractal and Guinier–Porod (GP) (Figure S3 in Supporting Information).[64,68,69] The mass fractal model calculates the scattering from fractal-like aggregates, which can be used to determine the size of scattering objects;[69] whereas, the GP model is an empirical model that calculates the scattering for a generalized Guinier/power law object, and can be used to determine the size and dimensionality of scattering objects, including asymmetric objects (such as rods or platelets), and shapes intermediate between spheres (globular) and rods or

DOI: 10.1021/acsami.8b20645
ACS Appl. Mater. Interfaces 2019, 11, 9934–9946

between rods and platelets.[68] The mass fractal model (Figure S3 in Supporting Information) did not give a satisfactory fit, when fixing the size of the building block to the known size of the carbon support (50 nm). Whereas freeing all parameters leads to a good fit but did not provide parameters with a reasonable physical meaning of the size/structure.[69] Among the tested models, the GP model (Figure 5A) was considered to be the most appropriate: even though the fits show some systematic deviations in the Guinier-like turnover region (Figure 5C), it picks up all the observed trends (intensity, Guinier-like turnover points, Porod slopes), and has only few parameters that are all physically meaningful. The difficulty in fitting the turn-over region could be attributed to high polydispersity in the system. Therefore, the absolute values for size from the fit parameters have to be taken with care, but trends are valid. In order to obtain the size of carbon aggregates, the scattering data of all samples were fitted with the GP model (Figures 5C, and S4 in Supporting Information) by fixing the Porod slope to 3.2 in order to have reduced fitting parameters, where all samples exhibited a Porod slope value of ∼3.2 estimated with the power law fit (discussed previously). The carbon aggregate sizes obtained from the data fits are given in Table 1. The R_g of carbon aggregates in catalyst ink prepared using partially deuterated 70% IPA/H_2O (Nafion contrast-matched) mixture as DM is ∼178.9 nm, which is in general agreement with values reported for alcohol-based catalyst ink dispersions.[23] A sequential reduction in IPA content in the catalyst ink dispersion resulted in progressive decrease in carbon aggregate R_g. Moreover, a dimension variable value, (Table 1) of ∼0.01 for all the samples suggests the carbon aggregate to be globular (Supporting Information eq. S2). The observed difference in carbon aggregate size with various IPA contents in DM is because of the change occurring in the carbon−carbon and carbon−Nafion ionomer intermolecular interactions. The hydrophobic carbon black can interact with Nafion ionomer NPs through both van der Waals and electrostatic forces, and the van der Waals force between Nafion ionomer and carbon black is reported to be dominant in alcohol-rich DMs.[28,51] Moreover, an increase in dielectric constant of DM increases the dependence of interaction energy on surface potential, where a higher value of interaction energy corresponds to higher stability of the ink.[51] Therefore, the results suggest that a decrease in IPA content in DM leads to a reduced absolute value of the ζ-potential of carbon black, an increased absolute value of the ζ-potential of Nafion ionomer NPs, and a decreased van der Waals force of attraction between carbon and Nafion ionomer in the catalyst ink, which in turn causes a decrease in carbon aggregate size stabilized by the Nafion ionomer.

Evolution of the Size and the Structure of Carbon Support-Nafion Ionomer Aggregate with Quality of DM. Figure 6 shows the double logarithmic SANS and USANS combined intensity profile of catalyst inks prepared using IPA/H_2O mixtures (without contrast-match) as DM, and their respective model function fits over a wide q-range (0.00007−0.3 Å^{-1}). Such plots enable elucidation of the size and structure of carbon aggregate−Nafion ionomer particles. The hydrogenated solvents in DM provide neutron SLD contrast against both the carbon support and the Nafion ionomer. The scattering intensity profile of the catalyst ink (Figure 6A) showed three distinctive regions: a high-q Porod region ($0.08 < q < 0.3$ Å^{-1}), a mid-q Porod region ($0.002 < q < 0.08$ Å^{-1}), and a low-q Guinier region ($0.00007 < q < 0.002$ Å^{-1}). The low-q Guinier region and mid-q Porod region are attributed to carbon aggregate−Nafion ionomer particles in the catalyst ink, whereas the high-q Porod region is dominated by Nafion ionomer NPs.[29] The scattering intensity of the catalyst ink was observed to decrease in the low-q region with a decrease in IPA content in DM. The decrease in low-q scattering intensity suggests a decrease in the size of carbon aggregate−Nafion ionomer particles. The concomitant increase in high-q scattering intensity suggests an increase in the size and scattering contribution (clearly seen in Kratky plot, Figure 6B) of Nafion ionomer NPs with a decrease in IPA content in DM. Moreover, the Kratky plot shows a slight shift in the peak maximum toward higher q-value supporting a decrease in the size of carbon aggregate−Nafion ionomer particles with decrease in IPA content in DM.[43,63] The mid-q scattering data ($0.006 < q < 0.02$ Å^{-1}) of the catalyst ink fitted with a power law function results in a slope value of ∼3.25 for all samples (Figure 6A), which is characteristic of surface fractals and is hypothesized to arise from carbon−Nafion−DM interface.[63] In order to obtain the structural parameters of carbon aggregate−Nafion ionomer particles in the catalyst ink, the high-q scattering data were fitted with the cylinder form factor (using structural parameters obtained from Nafion ionomer SANS data fit), whereas the mid-q and low-q scattering data were fitted with the GP model (Figure 6C−F) by fixing the Porod slope to 3.25 (Figure S5 in Supporting Information).[68] The combined form factor model function used for the catalyst ink data fit is given in eq 4

$$I(q) = A(q) + B(q) \tag{4}$$

where $A(q)$ is the GP model and $B(q)$ is the cylinder model.[64,68] The carbon aggregate−Nafion ionomer particle sizes obtained from the data fits are given in Table 1. The R_g of carbon aggregate−Nafion ionomer particles in the catalyst ink prepared using 70% IPA/H_2O mixture as DM was ∼191.9 nm, which is in general agreement with values reported for alcohol-based catalyst ink dispersions and is slightly higher than the R_g of carbon aggregates (∼178.9 nm) in the respective catalyst ink.[23] Therefore, the data indicate that the carbon aggregates are stabilized by a thin conformal layer of Nafion ionomer NPs forming a shell. An estimate of the thickness of the Nafion ionomer shell stabilizing the carbon aggregates may be obtained from the difference between the R_g of carbon aggregate−Nafion ionomer particles in the catalyst ink without contrast-match and carbon aggregate with Nafion contrast-match (Table 1). A sequential reduction in IPA content in the catalyst ink DM results in a decrease in the R_g of carbon aggregate−Nafion ionomer particles. On the basis of the established size of the Nafion ionomer NPs and estimated thickness of the Nafion ionomer shell, it is hypothesized that the carbon aggregates are stabilized by a few layers of Nafion ionomer NPs. The observed decrease in Nafion ionomer shell thickness in water-rich DMs may be because of increased electrostatic repulsion between Nafion ionomer NPs on carbon aggregate surfaces and decreased van der Waals force of attraction between carbon and Nafion ionomer NPs. The estimated Nafion ionomer shell thickness (∼13.0 nm for 70% IPA/H_2O mixture as DM) is in the range of values reported in the literature (4.5−15.0 nm for 80% IPA/H_2O mixture as DM,[17] and 6.0−8.0 nm for 66% IPA/H_2O mixture as DM.[30]) for the ECL. Variation in reported shell thickness may be attributed to the shrinkage of the Nafion ionomer shell during ECL fabrication (solvent removal or drying).[17,30]

Evolution of the Hierarchical Structure of Ionomer Shell with Quality of DM. To elucidate the hierarchical

DOI: 10.1021/acsami.8b20645
ACS Appl. Mater. Interfaces 2019, 11, 9934−9946

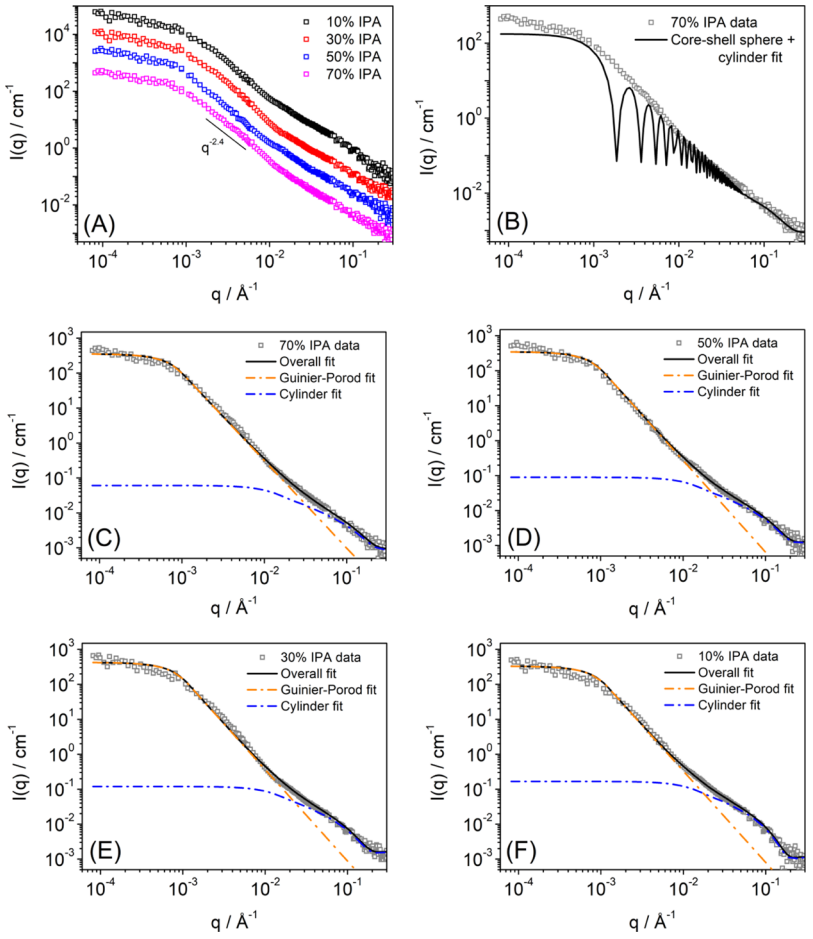

Figure 7. (A) Carbon contrast-matched SANS and USANS-combined intensity profile of fuel cell catalyst ink prepared using IPA-d/D_2O mixtures (carbon contrast-matched) as DM. The data are presented as intensity offsets for clarity. (B–F) are model function fits of respective scattering data.

structure of the Nafion ionomer in catalyst ink dispersions, SANS, and USANS measurements with carbon contrast-matching were performed. Figure 7 shows the double logarithmic SANS and USANS combined intensity profile of catalyst ink prepared using IPA-d/D_2O mixtures (carbon contrast-matched) as DM (dispersing solvent neutron SLD matched to carbon neutron SLD) and their respective model function fits. The scattering intensity profile of the Nafion ionomer (Figure 7A) within the experimental range shows three different q regions: a high-q Porod region ($0.01 < q < 0.36$ Å^{-1}), a mid-q Porod region ($0.001 < q < 0.01$ Å^{-1}), and a low-q Guinier region ($0.0007 < q < 0.001$ Å^{-1}). The high-q region corresponds to rodlike Nafion ionomer NPs, whereas mid-q and low-q regions correspond to the Nafion ionomer structure stabilizing carbon aggregates. Data fitting (Figures 7B, and S6 in Supporting Information) was attempted for catalyst ink prepared using 70% IPA-d/D_2O (carbon contrast-matched) mixture as DM with a combined form factor model function, similar to eq 4 using core–shell sphere model as A(q), and fixing structural parameters determined for Nafion ionomer NPs for B(q).[64,70] However, the fit did not converge (Figure 7B), suggesting the structure of catalyst ink to be not that of a simple core–shell particles in DM.[70] Moreover, the shape-independent power-law function fitted to mid-q scattering data ($0.0025 < q < 0.007$ Å^{-1}) returned a Porod slope value ~2.4 (Figure 7A), which is characteristic of mass fractals.[63] Therefore, it is hypothesized that the structure of the catalyst ink consists of randomly distributed carbon aggregates (core) stabilized by a thin layer of randomly distributed Nafion ionomer NPs (shell), and Nafion ionomer segments percolating through void spaces (primary pores) of carbon aggregates forming fractal connectivity.[13] In order to determine the structural parameters of the Nafion ionomer in the catalyst ink, the experimental scattering data were fitted (Figures 7C–F, and S7 in Supporting Information) with a combined form factor model function, as given in eq 4 using structural parameters determined for carbon aggregate–Nafion ionomer particles and pristine Nafion ionomer NPs. The obtained structural parameters of the Nafion ionomer in the catalyst ink are given in Table 1. The R_g of the Nafion ionomer structure forming the shell and percolating through carbon aggregates in the catalyst ink prepared using 70% IPA-d/D_2O mixture as DM was determined to be ~192.1 nm, which is in good agreement with the size determined for carbon aggregate–Nafion ionomer particles (Table 1). Moreover, the R_g of the Nafion ionomer structure forming the shell and percolating through carbon aggregates in the catalyst ink was shown to decrease with decrease in IPA content of DM, which supports a systematic change in carbon–ionomer interaction resulting in the observed size and structure change of the carbon aggregate–Nafion ionomer core–shell particles. A schematic illustration of the structure proposed for fuel cell catalyst inks prepared using IPA/H_2O mixtures as DM is presented in Figure 8.

DOI: 10.1021/acsami.8b20645
ACS Appl. Mater. Interfaces 2019, 11, 9934–9946

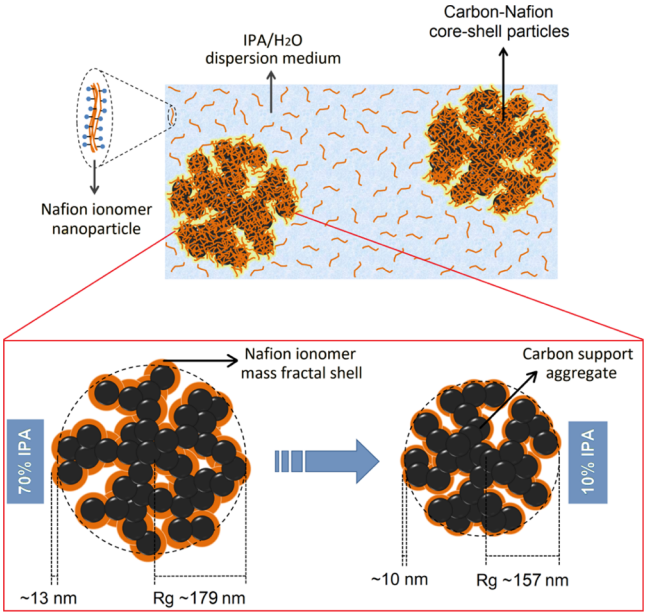

Figure 8. Schematic illustration of the colloidal structure of fuel cell catalyst ink prepared using IPA/H_2O mixtures as DM.

CONCLUSIONS

In this study, we have successfully established the colloidal structure of the fuel cell catalyst inks prepared using binary mixtures of IPA/H_2O as the DM using three different scattering approaches such as DLS, contrast-variation SANS and USANS. A variety of contrast-matching conditions have been used to elucidate the dimensions and morphology of the fuel cell catalyst assembly over a wide range of length scales. The structure of IPA/H_2O-based fuel cell catalyst ink dispersions is found to be randomly distributed particles of carbon aggregate−Nafion ionomer, which are distributed in the matrix of negatively surface charged rodlike (cylindrical) Nafion ionomer NPs. The ionomer shell stabilizing the carbon aggregates in the catalyst inks is observed to be mass fractal in nature. A progressive decrease in the alcohol content (or increasing water content) increases the dielectric constant of DM, which in turn increases the radius and electrostatic repulsion resulting from the increase in the ζ-potential of ionomer NPs. Consequently, with a systematic decrease in the alcohol content in DM, the dispersed ionomers become more dissociated, while the carbon aggregate structures in catalyst ink shrink with thinner ionomer shells. The results elucidate that changes in the interfacial structure via adjustments of DM composition can be used to control assembly morphology and ultimately tailor the structure-property relationship for colloidal fuel cell catalyst inks and provide a clear design pathway to further optimize the performance of the ECL. This work highlights the fundamental changes in the interfacial structure of the ECL ink formulations assembled in water-rich (green) DMs, which are believed to exhibit superior performance to their organic DM counterparts when casted into ECLs.

ASSOCIATED CONTENT

Supporting Information

The Supporting Information is available free of charge on the ACS Publications website at DOI: 10.1021/acsami.8b20645.

Explicit form of model functions used, and model fits and/or parameters obtained (PDF)

AUTHOR INFORMATION

Corresponding Authors

*E-mail: namita.choudhury@rmit.edu.au (N.R.C.).
*E-mail: naba.dutta@rmit.edu.au (N.K.D.).

ORCID

Naba K. Dutta: 0000-0003-4800-1910

Author Contributions

The manuscript was written through contributions of all authors. All authors have given approval to the final version of the manuscript.

Notes

The authors declare no competing financial interest.

ACKNOWLEDGMENTS

This work was financially supported by the Australian Research Council (ARC) Discovery grant (DP120103537). Access to the SANS and USANS facility at the ACNS was supported through ANSTO beam time award (P4033). The authors acknowledge the facilities, and the scientific and technical assistance, of the MicroNano Research Facility (MNRF) at the RMIT University, Melbourne. This work benefited from the use of the SasView application, originally developed under NSF award DMR-0520547. SasView contains code developed with funding from the European Union's Horizon 2020 research and innovation programme under the SINE2020 project, grant agreement no. 654000.

REFERENCES

(1) Wang, Y.; Chen, K. S.; Mishler, J.; Cho, S. C.; Adroher, X. C. A Review of Polymer Electrolyte Membrane Fuel Cells: Technology, Applications, and Needs on Fundamental Research. *Appl. Energy* **2011**, *88*, 981−1007.

(2) Therdthianwong, A.; Manomayidthikarn, P.; Therdthianwong, S. Investigation of Membrane Electrode Assembly (MEA) Hot-Pressing Parameters for Proton Exchange Membrane Fuel Cell. *Energy* **2007**, *32*, 2401−2411.

(3) O'Hayre, R.; Barnett, D. M.; Prinz, F. B. The Triple Phase Boundary: A Mathematical Model and Experimental Investigations for Fuel Cells. *J. Electrochem. Soc.* **2005**, *152*, A439−A444.

(4) Lobato, J.; Rodrigo, M. A.; Linares, J. J.; Scott, K. Effect of the Catalytic Ink Preparation Method on the Performance of High Temperature Polymer Electrolyte Membrane Fuel Cells. *J. Power Sources* **2006**, *157*, 284−292.

(5) Mehmood, A.; An, M.; Ha, H. Y. Tailoring Cathode Structure of Catalyst Coated Membranes for Performance Enhancement in Direct Methanol Fuel Cells. *Int. J. Hydrogen Energy* **2016**, *41*, 21366−21374.

(6) Zamel, N. The Catalyst Layer and its Dimensionality − A Look Into its Ingredients and How to Characterize their Effects. *J. Power Sources* **2016**, *309*, 141−159.

(7) Joachim, K.; Volker, B. Water-Based Catalyst Inks and their Use for Manufacture of Catalyst-Coated Substrates. U.S. Patent 20,040,023,104 A1, 2004.

(8) Xie, Z.; Zhao, X.; Adachi, M.; Shi, Z.; Mashio, T.; Ohma, A.; Shinohara, K.; Holdcroft, S.; Navessin, T. Fuel Cell Cathode Catalyst Layers From "Green" Catalyst Inks. *Energy Environ. Sci.* **2008**, *1*, 184−193.

(9) Howe, K. S.; Clark, E. R.; Bowen, J.; Kendall, K. A Novel Water-Based Cathode Ink Formulation. *Int. J. Hydrogen Energy* **2013**, *38*, 1731−1736.

(10) Ngo, T. T.; Yu, T. L.; Lin, H.-L. Influence of the Composition of Isopropyl Alcohol/Water Mixture Solvents in Catalyst Ink Solutions on Proton Exchange Membrane Fuel Cell Performance. *J. Power Sources* **2013**, *225*, 293−303.

DOI: 10.1021/acsami.8b20645
ACS Appl. Mater. Interfaces 2019, 11, 9934−9946

(11) Ngo, T. T.; Yu, T. L.; Lin, H.-L. Nafion-Based Membrane Electrode Assemblies Prepared From Catalyst Inks Containing Alcohol/Water Solvent Mixtures. *J. Power Sources* **2013**, *238*, 1−10.
(12) Takahashi, S.; Mashio, T.; Horibe, N.; Akizuki, K.; Ohma, A. Analysis of the Microstructure Formation Process and its Influence on the Performance of Polymer Electrolyte Fuel-Cell Catalyst Layers. *ChemElectroChem* **2015**, *2*, 1560−1567.
(13) Holdcroft, S. Fuel Cell Catalyst Layers: A Polymer Science Perspective. *Chem. Mater.* **2014**, *26*, 381−393.
(14) Mauritz, K. A.; Moore, R. B. State of Understanding of Nafion. *Chem. Rev.* **2004**, *104*, 4535−4586.
(15) Malek, K.; Mashio, T.; Eikerling, M. Microstructure of Catalyst Layers in PEM Fuel Cells Redefined: A Computational Approach. *Electrocatalysis* **2011**, *2*, 141−157.
(16) He, Q.; Suraweera, N. S.; Joy, D. C.; Keffer, D. J. Structure of the Ionomer Film in Catalyst Layers of Proton Exchange Membrane Fuel Cells. *J. Phys. Chem. C* **2013**, *117*, 25305−25316.
(17) Lopez-Haro, M.; Guétaz, L.; Printemps, T.; Morin, A.; Escribano, S.; Jouneau, P. H.; Bayle-Guillemaud, P.; Chandezon, F.; Gebel, G. Three-Dimensional Analysis of Nafion Layers in Fuel Cell Electrodes. *Nat. Commun.* **2014**, *5*, 5229.
(18) Paul, D. K.; Karan, K.; Docoslis, A.; Giorgi, J. B.; Pearce, J. Characteristics of Self-Assembled Ultrathin Nafion Films. *Macromolecules* **2013**, *46*, 3461−3475.
(19) Kim, J.-H.; Ha, H. Y.; Oh, I.-H.; Hong, S.-A.; Lee, H.-I. Influence of the Solvent in Anode Catalyst Ink on the Performance of a Direct Methanol Fuel Cell. *J. Power Sources* **2004**, *135*, 29−35.
(20) Fernández, R.; Ferreira-Aparicio, P.; Daza, L. PEMFC electrode preparation: Influence of the Solvent Composition and Evaporation Rate on the Catalytic Layer Microstructure. *J. Power Sources* **2005**, *151*, 18−24.
(21) Millington, B.; Du, S.; Pollet, B. G. The Effect of Materials on Proton Exchange Membrane Fuel Cell Electrode Performance. *J. Power Sources* **2011**, *196*, 9013−9017.
(22) Zhang, J. *PEM Fuel Cell Electrocatalysts and Catalyst Layers: Fundamentals and Applications*; Springer: London, 2008.
(23) Takahashi, S.; Shimanuki, J.; Mashio, T.; Ohma, A.; Tohma, H.; Ishihara, A.; Ito, Y.; Nishino, Y.; Miyazawa, A. Observation of Ionomer in Catalyst Ink of Polymer Electrolyte Fuel Cell Using Cryogenic Transmission Electron Microscopy. *Electrochim. Acta* **2017**, *224*, 178−185.
(24) Aldebert, P.; Dreyfus, B.; Pineri, M. Small-Angle Neutron Scattering of Perfluorosulfonated Ionomers in Solution. *Macromolecules* **1986**, *19*, 2651−2653.
(25) Yamaguchi, M.; Matsunaga, T.; Amemiya, K.; Ohira, A.; Hasegawa, N.; Shinohara, K.; Ando, M.; Yoshida, T. Dispersion of Rod-like Particles of Nafion in Salt-Free Water/1-Propanol and Water/Ethanol Solutions. *J Phys Chem B* **2014**, *118*, 14922−8.
(26) Kaler, E. W. Small-Angle Scattering From Colloidal Dispersions. *J. Appl. Crystallogr.* **1988**, *21*, 729−736.
(27) Xu, F.; Zhang, H.; Ilavsky, J.; Stanciu, L.; Ho, D.; Justice, M. J.; Petrache, H. I.; Xie, J. Investigation of a Catalyst Ink Dispersion Using Both Ultra-Small-Angle X-Ray Scattering and Cryogenic TEM. *Langmuir* **2010**, *26*, 19199−19208.
(28) Yang, F.; Xin, L.; Uzunoglu, A.; Qiu, Y.; Stanciu, L.; Ilavsky, J.; Li, W.; Xie, J. Investigation of the Interaction Between Nafion Ionomer and Surface Functionalized Carbon Black Using Both Ultrasmall Angle X-Ray Scattering and Cryo-TEM. *ACS Appl. Mater. Interfaces* **2017**, *9*, 6530−6538.
(29) Shibayama, M.; Matsunaga, T.; Kusano, T.; Amemiya, K.; Kobayashi, N.; Yoshida, T. SANS Studies on Catalyst Ink of Fuel Cell. *J. Appl. Polym. Sci.* **2014**, *131*, 39842.
(30) Kusano, T.; Hiroi, T.; Amemiya, K.; Ando, M.; Takahashi, T.; Shibayama, M. Structural Evolution of a Catalyst Ink for Fuel Cells During the Drying Process Investigated by CV-SANS. *Polym. J.* **2015**, *47*, 546−555.
(31) Balu, R.; Mata, J. P.; Knott, R.; Elvin, C. M.; Hill, A. J.; Choudhury, N. R.; Dutta, N. K. Effects of Crowding and Environment on the Evolution of Conformational Ensembles of the Multi-Stimuli-Responsive Intrinsically Disordered Protein, Rec1-Resilin: A Small-Angle Scattering Investigation. *J. Phys. Chem. B* **2016**, *120*, 6490−6503.
(32) Hollamby, M. J. Practical Applications of Small-Angle Neutron Scattering. *Phys. Chem. Chem. Phys.* **2013**, *15*, 10566−10579.
(33) Bhatia, S. R. Ultra-Small-Angle Scattering Studies of Complex Fluids. *Curr. Opin. Colloid Interface Sci.* **2005**, *9*, 404−411.
(34) Sze, A.; Erickson, D.; Ren, L.; Li, D. Zeta-Potential Measurement Using the Smoluchowski Equation and the Slope of the Current−Time Relationship in Electroosmotic Flow. *J. Colloid Interface Sci.* **2003**, *261*, 402−410.
(35) Dutta, N. K.; Choudhury, N. R.; Mayavan, S.; Balu, R.; Whittaker, J.; Elvin, C. M.; Hill, A. J. Template Directed Formation of Metal Nanoparticles and Uses Thereof. WO Patent 2014071463 A1, 2014.
(36) Balu, R.; Whittaker, J.; Dutta, N. K.; Elvin, C. M.; Choudhury, N. R. Multi-Responsive Biomaterials and Nanobioconjugates From Resilin-Like Protein Polymers. *J. Mater. Chem. B* **2014**, *2*, 5936−5947.
(37) Dutta, N. K.; Truong, M. Y.; Mayavan, S.; Roy Choudhury, N.; Elvin, C. M.; Kim, M.; Knott, R.; Nairn, K. M.; Hill, A. J. A Genetically Engineered Protein Responsive to Multiple Stimuli. *Angew. Chem., Int. Ed.* **2011**, *50*, 4428−4431.
(38) Dutta, N. K.; Choudhury, N. R.; Truong, M. Y.; Kim, M.; Elvin, C. M.; Hill, A. J. Physical Approaches for Fabrication of Organized Nanostructure of Resilin-Mimetic Elastic Protein Rec1-Resilin. *Biomaterials* **2009**, *30*, 4868−4876.
(39) Truong, M. Y.; Dutta, N. K.; Choudhury, N. R.; Kim, M.; Elvin, C. M.; Hill, A. J.; Thierry, B.; Vasilev, K. A pH-Responsive Interface Derived From Resilin-Mimetic Protein Rec1-Resilin. *Biomaterials* **2010**, *31*, 4434−4446.
(40) Balu, R.; Knott, R.; Cowieson, N. P.; Elvin, C. M.; Hill, A. J.; Choudhury, N. R.; Dutta, N. K. Structural Ensembles Reveal Intrinsic Disorder for the Multi-Stimuli responsive Bio-Mimetic Protein Rec1-Resilin. *Sci. Rep.* **2015**, *5*, 10896.
(41) Elvin, C. M.; Carr, A. G.; Huson, M. G.; Maxwell, J. M.; Pearson, R. D.; Vuocolo, T.; Liyou, N. E.; Wong, D. C. C.; Merritt, D. J.; Dixon, N. E. Synthesis and Properties of Crosslinked Recombinant Pro-Resilin. *Nature* **2005**, *437*, 999−1002.
(42) Wood, K.; Mata, J. P.; Garvey, C. J.; Wu, C.-M.; Hamilton, W. A.; Abbeywick, P.; Bartlett, D.; Bartsch, F.; Baxter, P.; Booth, N.; Brown, W.; Christoforidis, J.; Clowes, D.; d'Adam, T.; Darmann, F.; Deura, M.; Harrison, S.; Hauser, N.; Horton, G.; Federici, D.; Franceschini, F.; Hanson, P.; Imamovic, E.; Imperia, P.; Jones, M.; Kennedy, S.; Kim, S.; Lam, T.; Lee, W. T.; Lesha, M.; Mannicke, D.; Noakes, T.; Olsen, S. R.; Osborn, J. C.; Penny, D.; Perry, M.; Pullen, S. A.; Robinson, R. A.; Schulz, J. C.; Xiong, N.; Gilbert, E. P. QUOKKA, the Pinhole Small-Angle Neutron Scattering Instrument at the OPAL Research Reactor, Australia: Design, Performance, Operation and Scientific Highlights. *J. Appl. Crystallogr.* **2018**, *51*, 294−314.
(43) Lipfert, J.; Doniach, S. Small-Angle X-Ray Scattering From RNA, Proteins, and Protein Complexes. *Annu. Rev. Biophys. Biomol. Struct.* **2007**, *36*, 307−327.
(44) Kline, S. R. Reduction and Analysis of SANS and USANS Data Using IGOR Pro. *J. Appl. Crystallogr.* **2006**, *39*, 895−900.
(45) Konarev, P. V.; Volkov, V. V.; Sokolova, A. V.; Koch, M. H. J.; Svergun, D. I. PRIMUS: A Windows PC-Based System for Small-Angle Scattering Data Analysis. *J. Appl. Crystallogr.* **2003**, *36*, 1277−1282.
(46) Rehm, C.; de Campo, L.; Brûlé, A.; Darmann, F.; Bartsch, F.; Berry, A. Design and Performance of the Variable-Wavelength Bonse-Hart Ultra-Small-Angle Neutron Scattering Diffractometer KOOKA-BURRA at ANSTO. *J. Appl. Crystallogr.* **2018**, *51*, 1−8.
(47) Balu, R.; Reeder, S.; Knott, R.; Mata, J.; de Campo, L.; Dutta, N. K.; Choudhury, N. R. Tough Photocrosslinked Silk Fibroin/Graphene Oxide Nanocomposite Hydrogels. *Langmuir* **2018**, *34*, 9238−9251.
(48) Akerlof, G. Dielectric Constants of Some Organic Solvent-Water Mixtures at Various Temperatures. *J. Am. Chem. Soc.* **1932**, *54*, 4125−4139.
(49) Vazquez, G.; Alvarez, E.; Navaza, J. M. Surface Tension of Alcohol Water + Water From 20 to 50 °C. *J. Chem. Eng. Data* **1995**, *40*, 611−614.

DOI: 10.1021/acsami.8b20645
ACS Appl. Mater. Interfaces 2019, 11, 9934−9946

(50) Schmidt-Rohr, K.; Chen, Q. Parallel Cylindrical Water Nanochannels in Nafion Fuel-Cell Membranes. *Nat. Mater.* **2007**, *7*, 75−83.
(51) Shukla, S.; Bhattacharjee, S.; Weber, A. Z.; Secanell, M. Experimental and Theoretical Analysis of Ink Dispersion Stability for Polymer Electrolyte Fuel Cell Applications. *J. Electrochem. Soc.* **2017**, *164*, F600−F609.
(52) Kreuer, K. D. On the Development of Proton Conducting Polymer Membranes for Hydrogen and Methanol Fuel Cells. *J. Membr. Sci.* **2001**, *185*, 29−39.
(53) Lee, S.-J.; Yu, T. L.; Lin, H.-L.; Liu, W.-H.; Lai, C.-L. Solution Properties of Nafion in Methanol/Water Mixture Solvent. *Polymer* **2004**, *45*, 2853−2862.
(54) Duan, Q.; Wang, H.; Benziger, J. Transport of Liquid Water Through Nafion Membranes. *J. Membr. Sci.* **2012**, *392*−*393*, 88−94.
(55) Loppinet, B.; Gebel, G.; Williams, C. E. Small-Angle Scattering Study of Perfluorosulfonated Ionomer Solutions. *J. Phys. Chem. B* **1997**, *101*, 1884−1892.
(56) Jiang, S.; Xia, K.-Q.; Xu, G. Effect of Additives on Self-Assembling Behavior of Nafion in Aqueous Media. *Macromolecules* **2001**, *34*, 7783−7788.
(57) Zhang, H.; Pan, J.; He, X.; Pan, M. Zeta Potential of Nafion Molecules in Isopropanol-Water Mixture Solvent. *J. Appl. Polym. Sci.* **2008**, *107*, 3306−3309.
(58) Xu, R.; Wu, C.; Xu, H. Particle Size and Zeta Potential of Carbon Black in Liquid Media. *Carbon* **2007**, *45*, 2806−2809.
(59) Rivin, D. Surface Properties of Carbon. *Rubber Chem. Technol.* **1971**, *44*, 307−343.
(60) Chen, S. H.; Huang, J. S.; Tartaglia, P. *Structure and Dynamics of Strongly Interacting Colloids and Supramolecular Aggregates in Solution*; Springer: Netherlands, 2012.
(61) Feigin, L. A.; Svergun, D. I. *Structure Analysis by Small-Angle X-Ray and Neutron Scattering*; Springer: US, 2013.
(62) Putnam, C. D.; Hammel, M.; Hura, G. L.; Tainer, J. A. X-Ray Solution Scattering (SAXS) Combined With Crystallography and Computation: Defining Accurate Macromolecular Structures, Conformations and Assemblies in Solution. *Q. Rev. Biophys.* **2007**, *40*, 191−285.
(63) Glatter, O.; Kratky, O. *Small Angle X-ray Scattering*; Academic Press: New York, 1982.
(64) Pedersen, J. S. Analysis of Small-Angle Scattering Data from Colloids and Polymer Solutions: Modeling and Least-Squares Fitting. *Adv. Colloid Interface Sci.* **1997**, *70*, 171−210.
(65) Welch, C.; Labouriau, A.; Hjelm, R.; Orler, B.; Johnston, C.; Kim, Y. S. Nafion in Dilute Solvent Systems: Dispersion or Solution? *ACS Macro Lett.* **2012**, *1*, 1403−1407.
(66) Whittaker, J. L.; Balu, R.; Knott, R.; de Campo, L.; Mata, J. P.; Rehm, C.; Hill, A. J.; Dutta, N. K.; Roy Choudhury, N. Structural Evolution of Photocrosslinked Silk Fibroin and Silk Fibroin-Based Hybrid Hydrogels: A Small Angle and Ultra-Small Angle Scattering Investigation. *Int. J. Biol. Macromol.* **2018**, *114*, 998−1007.
(67) Ferraro, G.; Fratini, E.; Rausa, R.; Fiaschi, P.; Baglioni, P. Multiscale Characterization of some Commercial Carbon Blacks and Diesel Engine Soot. *Energy Fuels* **2016**, *30*, 9859−9866.
(68) Hammouda, B. New Guinier-Porod Model. *J. Appl. Crystallogr.* **2010**, *43*, 716−719.
(69) Mildner, D. F. R.; Hall, P. L. Small-Angle Scattering From Porous Solids with Fractal Geometry. *J. Phys. D: Appl. Phys.* **1986**, *19*, 1535−1545.
(70) Guinier, A.; Fournet, G. *Small-Angle Scattering of X-Rays*; Wiley: New York, 1955.

DOI: 10.1021/acsami.8b20645
ACS Appl. Mater. Interfaces 2019, 11, 9934−9946